Analysis of the xuv photoabsorption spectrum of Au^{2+}, Au^{3+}, and Au^{4+}

M. G. Su and C. Z. Dong*
College of Physics and Electronic Engineering, Northwest Normal University, Lanzhou 730070, China and Joint Laboratory of Atomic and Molecular Physics, NWNU & IMP CAS, Lanzhou 730070, China

N. Murphy and G. O'Sullivan
School of Physics, University College Dublin, Belfield, Dublin 4, Ireland
(Received 25 October 2008; published 20 April 2009)

The photoabsorption processes of Au^{2+}, Au^{3+}, and Au^{4+} have been investigated experimentally and theoretically in the 70–127 eV region. Using the dual laser-produced plasma technique, the $4f$ and $5p$ photoabsorption spectrum has been recorded at 50 ns time delay and was found to be dominated by a great number of lines from $4f$-$5d$, $6d$ and $5p$-$5d$, $6s$ transitions, which have been identified by comparison with the aid of Hartree-Fock with configuration interaction calculations. The characteristic feature of the spectrum is that satellite lines from excited configurations containing one or two $6s$ electrons are more important than resonance lines, and with increasing ionization, satellite contributions from states with one $6s$ spectator electron gradually become more important than those with two $6s$ spectator electrons. Based on the assumption of a normalized Boltzmann distribution among the excited states and a steady-state collisional-radiative model, we succeeded in reproducing a spectrum which is in good agreement with experiment.

DOI: 10.1103/PhysRevA.79.042507 PACS number(s): 32.30.Jc, 32.80.Hd

I. INTRODUCTION

In recent years, gold has been the subject of much research because of its considerable interest in indirectly driven inertial confinement fusion (ICF) [1–4], where laser radiation heats the inside of a gold hohlraum producing a plasma that emits intense x rays. The x-ray radiation drives the capsule implosion and influences the resulting fusion yield. On the other hand, gold is the last member of the $5d$ transition metal series which has a filled $5d$ subshell. The simple term structure of the $4f$ and $5p$ excitations of atomic gold and its low charged ions makes it an ideal representative of the heavier elements for the study of electron correlations and relativistic effects.

Several experimental and theoretical works on the $4f$ and $5p$ excitation spectra of the $5d$ transition metals have been carried out in the past years. Haensel *et al.* [5] first systematically studied the photoabsorption spectra in the xuv energy region of the $5d$ transition metals Ta, W, Re, Pt, and Au and observed two strong and broad absorption features that originate from excitation of $5p$ subshell electrons but only transition lines from $4f$ subshell of Pt. With the aim of studying correlation and relativistic effects, Costello *et al.* [6] also carried out inner-shell photoabsorption studies for W and Pt. Using the dual laser-produced plasma (DLP) technique, they recorded the absorption spectra of atomic W and Pt in the energy range of the $4f$ and $5p$ excitations and found that similar broad, strong, and asymmetric $5p$-$5d$ resonances dominate the spectra while the $4f$-$5d$ transitions give rise to prominent maxima superimposed on the high energy slope of the $5p$-$5d$ resonances. Köble *et al.* [7] studied the photoabsorption spectrum of atomic Au in the $4f$ and $5p$ excitation region again using the same DLP technique and compared their results with spectra calculated with the Hartree-Fock method and the relativistic time dependent local density approximation [8]. They found that the observed spectrum is dominated by two prominent Fano-type resonance lines which can be attributed to $5p$-$5d$ and $4f$-$5d$ transitions of valence-excited $5d^9 6s^2(^2D_{5/2})$ Au followed by autoionization.

From the foregoing experimental and theoretical work it is seen that the spectrum of atomic gold in the xuv range does not consist of sharp and well separated features. However, up to now, for the higher charged gold ions no supporting experimental data and theoretical results are available. Once the $5d$ subshell is open, one expects to see some strong and broad quasicontinuous peaks that include perhaps thousands of individual lines which merge to form such features. Therefore, it is necessary to obtain detailed information on the positions and intensities of lines from each stage in order to explain their origin.

In this paper we report a photoabsorption spectrum recorded using the DLP method in the 70–127 eV energy region and present the results of systematic calculations for $4f$ and $5p$ excitations in Au^{2+}, Au^{3+}, and Au^{4+} ions. The combination of experimental results and theoretical calculations has provided a calibration of the theory which is used to identify the $5d$ inner-shell excited spectrum of Au^{2+}, Au^{3+}, and Au^{4+} ions and to make further predictions for the decay pathways. Here, we will give a brief description of our theoretical analysis and present calculated cross sections for each ion in Sec. III and give a comparison between theoretical and experimental spectra in Sec. IV.

II. EXPERIMENT

Photoabsorption spectra of Au^{2+}, Au^{3+}, and Au^{4+} ions were recorded photoelectrically on a 0.25 m Jenoptic E-Spec flat field spectrograph using the DLP method. The spectrum

*Corresponding author; dongcz@nwnu.edu.cn

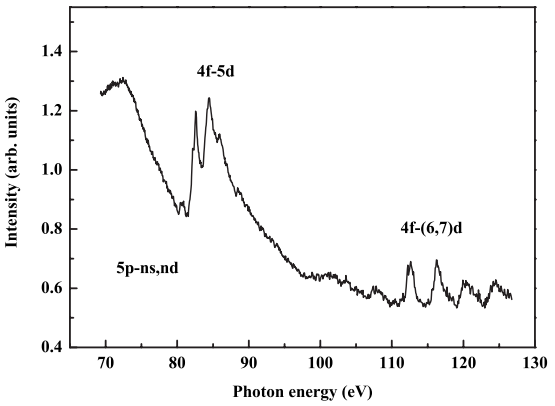

FIG. 1. Photoabsorption spectrum from laser-produced gold plasmas recorded with the DLP technique at 50 ns time delay.

was recorded on a back thinned intensity calibrated 1024 $\times$1024 pixel charge-coupled device (CCD) detector whose position is fixed and gives a simultaneous energy coverage from 70 to 127 eV. Details of the experimental setup and DLP technique have already been reported [9,10], and only a brief description is presented here.

In the present experiments, a 700 mJ, 15 ns full width at half maximum (FWHM), 1.06 μm Nd:YAG laser pulse was used to provide the backlighting continuum by tightly focusing onto a tungsten target while the absorbing plasma was produced by a similar Nd:YAG laser pulse, focused through a spherical lens to produce a damage area approximately 0.5 mm in diameter on a planar gold target. The plasma conditions were altered by either varying the laser pulse energy while maintaining tight focus or keeping the laser energy fixed and changing the focusing conditions since the plasma electron temperature and hence the degree of ionization are sensitive functions of the laser pulse power density. Using the full laser pulse energy of 900 mJ yielded an average power density ϕ of 1.2×10^9 W cm^{-2}.

Data files were provided with the spectrometer giving λ, $\Delta\lambda$, and counts per photon for each row of the CCD array giving a resolving power $E/\Delta E$ between 1300 and 1900 (with decreasing energy). The emission intensity of the backlighting plasma (I_0) was recorded before the acquisition of each absorption spectrum (I) to ensure that there was no shot-to-shot variation due to fluctuations in laser pulse energy and/or focusing conditions and to correct for any nonuniformity of the spectrograph and detector spectral response. The relative absorption cross section was then obtained from $\ln(I/I_0)$ and thus the absorption spectrum represents the overall relative spectral variation in the absorption of the plasma to an energy accuracy of within 0.05 eV. The overall energy uncertainty corresponds to three pixels of the CCD array. The spectrum was calibrated by superimposing emission lines from an aluminum plasma.

The gold photoabsorption spectrum in the 70–127 eV photon energy region is presented in Fig. 1. The spectrum recorded at 50 ns time delay was recorded from a location close to the target surface. There are two broad and asymmetric features and a smooth and monotonically decreasing slope in the 78–100 eV region; the experimental features observed in the 78–95 eV photon energy range have a sharp asymmetric structure which is very similar to the structure of Pt I observed by Costello *et al.* [6]. Below 78 eV a broad and strong peak at 72.43 eV is also in evidence. However measurements at lower energies were not possible due to the limitation of range available with the spectrometer.

III. ATOMIC STRUCTURE CALCULATIONS

In order to identify the structures of the experimental spectra, a series of calculations was performed with the Cowan RCN, RCN2, and RCG suites of Hartree-Fock with configuration interaction (HFCI) codes [11]. Due to the near degeneracy of the 5*d* and 6*s* orbitals, the initial states were calculated with the configurations $5p^64f^{14}5d^k$, $5p^64f^{14}5d^{k-1}6s$, and $5p^64f^{14}5d^{k-2}6s^2$ to account for configuration interaction. (Note that $k=9$ for Au^{2+}, $k=8$ for Au^{3+}, and $k=7$ for Au^{4+}.) The energy levels, weighted oscillator strengths, and linewidths were determined in a CI calculation using an excited state basis containing $5p^64f^{13}5d^knd$, $5p^64f^{13}5d^{k-1}6snd$, $5p^64f^{13}5d^{k-2}6s^2nd$, $5p^54f^{14}5d^knd$, $5p^54f^{14}5d^{k-1}6snd$, and $5p^54f^{14}5d^{k-2}6s^2nd$ states with n ($5\leq n\leq 8$) and discretized continuum states for a range of energies up to 6.9 and 5.1 Ry above the 4*f* and 5*p* ionization threshold, respectively. In all of these calculations, in order to optimize the output of the Cowan code, the Slater-Condon integrals (F^k, G^k, and R^k) were reduced to 85% to account for interaction with high-lying configurations omitted from the calculation while the spin parameter (ζ) was retained. All of the initial- and final-state configurations included in the calculations were summarized in Table I.

In the present calculations, the ground configuration of Au ions from Au^{2+} to Au^{4+} possesses an open 5*d* subshell, and the excited configurations contain open 4*f*, 5*p*, 6*s*, and/or *nd* ($5\leq n\leq 8$) subshells, so there exist a large number of near-degenerate energy levels when they couple with the electrons of other shells. Transitions between such complex configurations yield a great number of lines. Simultaneously, these lines are broadened by the interaction with the $5d$-εl ionization continuum through autoionization involving 4*f* and 5*p* electrons. As a result, with increasing ionization, the spectra resulting from the transitions between these levels become increasingly complex. For clarity, as an example, Fig. 2 shows the energy level structures connected with the 4*f* and 5*p* excitations and the corresponding Auger decays of Au^{3+} ions. Levels are indicated by the configuration average energy $E_{\rm av}$ and width ΔE. ΔE is the sum of the level statistical width ΔE_r and the configuration average autoionization width $\Gamma_{\rm av}$, where

$$\Delta E_r = \sqrt{\frac{\sum[(g_i f_{ij})(E_{ij}-E_{\rm av})^2]}{\sum(g_i f_{ij})}},$$

$$\Gamma_{\rm av} = \hbar \bar{A}^a.$$

In constructing the absorption cross sections, the discrete features were assumed to have a Lorentzian profile [11] and the resonant part of the cross sections (in Mb) were calculated using

TABLE I. Initial- and final-state configurations included in the calculations. In the designations of the configuration, $k=9$ for Au^{2+}, $k=8$ for Au^{3+}, and $k=7$ for Au^{4+}, where n is taken from 5 to 8.

		Final states	
Initial states	Excitation types	Discrete	Continuum
$5p^64f^{14}5d^k$	$4f$	$5p^64f^{13}5d^knd$	$5p^64f^{14}5d^{k-2}nd+\varepsilon(p,f,h,k)$
$5p^64f^{14}5d^{k-1}6s$			$5p^64f^{14}5d^{k-3}6snd+\varepsilon(p,f,h,k)$
$5p^64f^{14}5d^{k-2}6s^2$			$5p^64f^{14}5d^{k-4}6s^2nd+\varepsilon(p,f,h,k)$
		$5p^64f^{13}5d^{k-1}6snd$	$5p^64f^{14}5d^{k-2}nd+\varepsilon(p,f,h)$
			$5p^64f^{14}5d^{k-3}6snd+\varepsilon(p,f,h)$
		$5p^64f^{13}5d^{k-2}6s^2nd$	$5p^64f^{14}5d^{k-2}nd+\varepsilon f$
	$5p$	$5p^54f^{14}5d^knd$	$5p^64f^{14}5d^{k-2}nd+\varepsilon(p,f,h)$
			$5p^64f^{14}5d^{k-3}6snd+\varepsilon(p,f,h)$
			$5p^64f^{14}5d^{k-4}6s^2nd+\varepsilon(p,f,h)$
		$5p^54f^{14}5d^{k-1}6snd$	$5p^64f^{14}5d^{k-2}nd+\varepsilon(p,f)$
			$5p^64f^{14}5d^{k-3}6snd+\varepsilon(p,f)$
		$5p^54f^{14}5d^{k-2}6s^2nd$	$5p^64f^{14}5d^{k-2}nd+\varepsilon p$

$$\sigma = 109.7\Gamma_k f_k[2\pi(E_k - E)^2 + \Gamma_k^2/4]^{-1}, \quad (1)$$

where E_k and Γ_k are the calculated energy and calculated linewidth of the transition with energy E_k (in eV) and f_k is the absorption oscillator strength. To calculate σ it is therefore necessary to evaluate autoionization widths, Γ_k, which were calculated by summing contributions from the allowed nonradiative decay processes.

To compare the experimental spectra with the calculated cross sections for a given set of transitions from different charge states, the individual lines calculated were also directly convolved with a Gaussian function of FWHM of 0.05 eV corresponding to the instrumental resolution of the flat field spectrometer to produce a theoretical line spectrum for each ion stage. Both these line spectra and the theoretical cross sections were used to aid the identification of the origin of the resonance structures in the measured spectra. In Secs. III A and III B, the cross section of each ion stage is displayed with black lines while the theoretical line spectra are shown as gray lines.

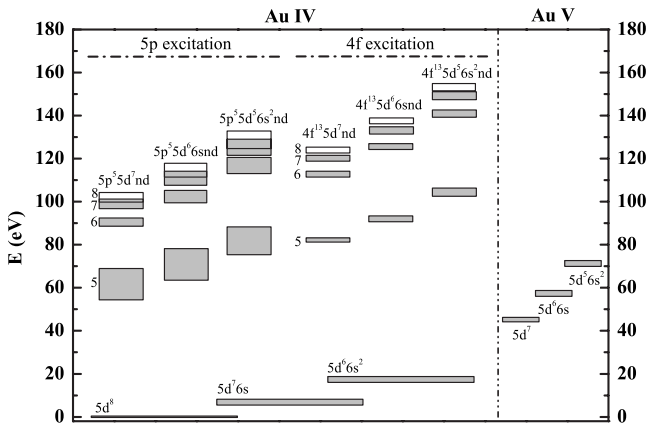

FIG. 2. Energy level diagram connected with the $4f$ and $5p$ excitations and the corresponding Auger decays of Au^{3+}.

A. $4f$ excitations

Figure 3 shows the calculated cross sections and convolved spectra of $4f$-nd ($n=5,6$) transition arrays from Au^{2+} to Au^{4+} ions. From this figure it is clear that there are very similar spectral features. In the $4f$-$5d$ region, in contrast to the atomic gold case [7] their profiles are not Fano type but with increasing ionization forms a broad band whose widths exceed 4.3 eV. Table II shows the corresponding summarized data, such as energy range, number of lines, sum of gf values, sum of weighted radiation probabilities, sum of

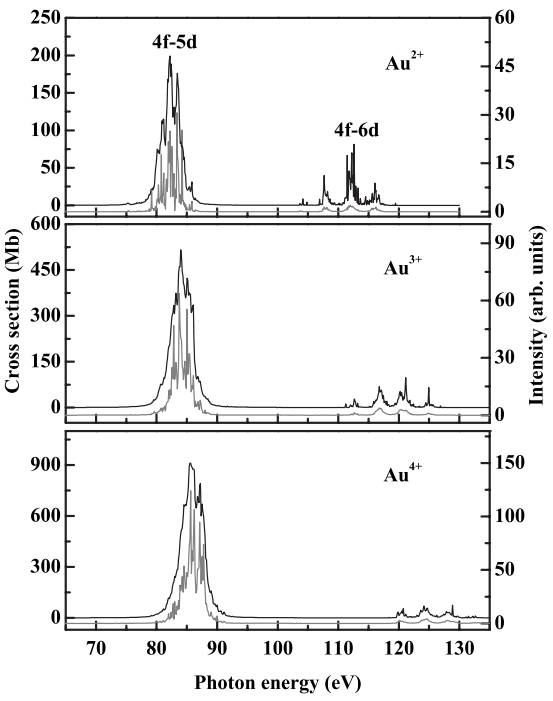

FIG. 3. Comparison between theoretical contributions of photoabsorption cross section (black lines) and line intensity (gray lines) due to $4f$-$5d$, $6d$ transition array of Au^{2+}, Au^{3+}, and Au^{4+}.

TABLE II. Summarized data which contain energy range, number of lines (N), sum of gf values (Σgf), sum of weighted radiation probabilities (ΣgA^r), sum of weighted autoionization probabilities (ΣgA^a), configuration average autoionization probabilities ($\bar{A}^a$), and average linewidths ($\bar{\Gamma}$) of individual line in the $4f$-$5d$ transitions from Au^{2+}, Au^{3+}, and Au^{4+} ions. Numbers in brackets denote powers of 10.

Ions	Transition array	Energy range (eV)	N	Σgf	ΣgA^r (s^{-1})	ΣgA^a (s^{-1})	$\bar{A}^a$ (s^{-1})	$\bar{\Gamma}$ (eV)
Au^{2+}	$4f^{14}5d^9$-$4f^{13}5d^{10}$	79.56–83.23	3	0.70	1.98[11]	1.58[16]	7.89[14]	0.078
	$4f^{14}5d^86s$-$4f^{13}5d^{10}$	71.29–78.18	9	0.02	4.30[09]	4.89[16]	7.89[14]	0.075
	$4f^{14}5d^9$-$4f^{13}5d^96s$	83.99–92.24	23	0.03	1.02[10]	6.77[16]	4.98[14]	0.054
	$4f^{14}5d^86s$-$4f^{13}5d^96s$	74.52–87.46	279	13.24	3.85[12]	8.87[17]	5.04[14]	0.051
	$4f^{14}5d^76s^2$-$4f^{13}5d^96s$	68.48–80.40	106	0.07	1.74[10]	3.63[17]	5.11[14]	0.049
	$4f^{14}5d^9$-$4f^{13}5d^86s^2$	92.84–102.21	24	0.01	2.39[09]	3.69[16]	2.63[14]	0.029
	$4f^{14}5d^86s$-$4f^{13}5d^86s^2$	82.52–96.69	201	0.14	4.96[10]	3.40[17]	2.56[14]	0.025
	$4f^{14}5d^76s^2$-$4f^{13}5d^86s^2$	74.07–92.44	654	27.29	8.22[12]	1.05[18]	2.41[14]	0.024
Au^{3+}	$4f^{14}5d^8$-$4f^{13}5d^9$	76.08–87.26	75	6.74	1.98[12]	3.23[17]	6.99[14]	0.072
	$4f^{14}5d^76s$-$4f^{13}5d^9$	67.79–78.63	123	0.05	1.23[10]	5.59[17]	6.66[14]	0.063
	$4f^{14}5d^8$-$4f^{13}5d^86s$	85.96–98.38	208	0.11	3.85[10]	5.73[17]	4.17[14]	0.041
	$4f^{14}5d^76s$-$4f^{13}5d^86s$	74.24–90.45	2297	55.50	1.69[13]	6.30[18]	4.06[14]	0.039
	$4f^{14}5d^66s^2$-$4f^{13}5d^86s$	66.70–80.19	347	0.09	2.26[10]	1.09[18]	4.17[14]	0.036
	$4f^{14}5d^8$-$4f^{13}5d^76s^2$	99.95–111.33	46	0.01	3.91[09]	8.27[16]	2.28[14]	0.019
	$4f^{14}5d^76s$-$4f^{13}5d^76s^2$	85.53–103.59	683	0.23	8.92[10]	1.04[18]	2.04[14]	0.018
	$4f^{14}5d^66s^2$-$4f^{13}5d^76s^2$	72.91–95.26	2355	66.33	2.10[13]	3.26[18]	1.96[14]	0.018
Au^{4+}	$4f^{14}5d^7$-$4f^{13}5d^8$	75.89–88.01	647	28.25	8.72[12]	2.25[18]	5.20[14]	0.051
	$4f^{14}5d^66s$-$4f^{13}5d^8$	68.08–77.17	293	0.07	1.58[10]	1.29[18]	5.46[14]	0.044
	$4f^{14}5d^7$-$4f^{13}5d^76s$	88.29–102.47	651	0.17	7.11[10]	1.61[18]	3.26[14]	0.029
	$4f^{14}5d^66s$-$4f^{13}5d^76s$	73.98–93.41	8462	134.89	4.33[13]	1.92[19]	3.15[14]	0.029
	$4f^{14}5d^56s^2$-$4f^{13}5d^76s$	68.99–78.75	336	0.06	1.50[10]	9.57[17]	3.23[14]	0.024
	$4f^{14}5d^7$-$4f^{13}5d^66s^2$	109.73–119.18	40	0.01	3.62[09]	7.17[16]	1.81[14]	0.012
	$4f^{14}5d^66s$-$4f^{13}5d^66s^2$	85.09–108.43	969	0.22	9.61[10]	1.22[18]	1.51[14]	0.012
	$4f^{14}5d^56s^2$-$4f^{13}5d^66s^2$	76.58–96.54	4364	103.25	3.45[13]	4.93[18]	1.55[14]	0.014

weighted autoionization probabilities, configuration average autoionization probabilities, and average linewidths of individual line in the $4f$-$5d$ transitions from Au^{2+}, Au^{3+}, and Au^{4+} ions. From Table II, we can find that there are eight transition arrays for each ion, every transition array covers an extended energy range and overlaps each other. By comparison with the sum of gf values among the transition arrays from different ionized gold ions, we find that in the $4f$ excitation region transitions of the types $4f^{14}5d^k$-$4f^{13}5d^{k+1}$, $4f^{14}5d^{k-1}6s$-$4f^{13}5d^k6s$, and $4f^{14}5d^{k-2}6s^2$-$4f^{13}5d^{k-1}6s^2$ predominate. The first type is a $4f$-$5d$ resonant transition, while the latter two can be regarded as satellite transitions with one and two $6s$ spectator electrons. For simplicity, transitions can be simplified to the following types, $4f^{13}5d^k(4f$-$5d)$, $4f^{13}5d^{k-1}(4f$-$5d)6s$, and $4f^{13}5d^{k-2}(4f$-$5d)6s^2$. In comparison to the above three transitions, the remaining five transitions considered are much weaker and can be neglected. Furthermore, the satellite lines from configurations with one and two $6s$ electrons are more important than resonance lines, and with increasing ionization, satellite contributions with one $6s$ spectator electron gradually become more important than that with two $6s$ spectator electrons. As is indicated in Fig. 3, the line groups from different transition arrays encountered blend to form a narrow band of quasicontinuum near 82 eV, and with increasing ionization this band gradually moves to higher energy. In addition, looking at the average linewidths ($\bar{\Gamma}$), we find that the linewidths of resonant lines are comparable to the instrumental resolution, while those of satellite lines are less than the instrumental resolution.

In contrast to $4f$-$5d$ transitions, the $4f$-$6d$ transition arrays cover a much wider energy span and are shifted to the higher energy side of $4f$ excitation region. Here we first calculated the transitions of the types $4f^{13}5d^k(4f$-$6d)$, $4f^{13}5d^{k-1}(4f$-$6d)6s$, and $4f^{13}5d^{k-2}(4f$-$6d)6s^2$. To explain the origin of the well-defined unresolved transition arrays (UTA) peaks, we analyze the distributions of the transition lines from the different Au ions. We find that each type of transition array consists of two groups of lines due to the coupling between the $4f$ and $6d$ electrons. In addition, among the positions of these six groups of lines there is the very interesting observation that the second group of lines from the first transition array overlaps almost perfectly the first group of lines from the second transition array so as to form a "bunch" of four UTA peaks. The overlapped two UTA peaks are, as a consequence, stronger than others. As is indicated in

Fig. 3, thousands of weak lines from the $4f$-$6d$ transition arrays lie above 95 eV so that each transition group is localized within an energy range of about 20 eV. They combine to yield a series of UTA peaks whose energy intervals between them are about 4 eV. These spectral features bear a strong resemblance to the structure from 95 to 125 eV in Fig. 1 which consists of five broad and intense continuumlike peaks. Köble *et al.* [7] observed some similar line structure in the 100 eV energy region. However, they gave no definite explanation because of the lack of information on the spectra from higher ionization stages but found that by shortening the time delay between the laser pulses, their relative intensity changed in tandem with the characteristic $4f$-$5d$ line of Au. They therefore concluded that these lines arose from the $4f$-$6d$ transition. Moreover, by comparison between the measured spectrum and calculated absorption cross section in the $4f$-$6d$ region from Au^{2+} to Au^{4+} ions, it was necessary to shift the computed cross sections to lower energy by 1.9 eV to obtain better agreement between experiment and calculation, presumably due to the omission of higher excited states because of the limitation of computer memory. We can however be sure that those UTA peaks in the experimental spectra arise from the contributions of mixtures of Au^{2+}, Au^{3+}, Au^{4+}, or higher charged gold ions.

In addition, for the transition arrays of $4f$-nd $(n \geq 7)$, there are similar spectral features. With increasing n, their position shifted lightly to higher energy but their intensities were so low that it was decided to exclude them from the calculations.

B. 5*p* excitations

The same procedure was next used to predict the $5p$ absorption spectral features of Au^{2+}, Au^{3+}, and Au^{4+} ions. Figure 4 shows the theoretically calculated cross sections and convolved spectra of $5p$-$5d$ transition arrays. The corresponding summarized data are shown in Table III.

Compared with Table II, we find the following differences in Table III: (1) transitions of the type $5p^6 4f^{14} 5d^{k-2} 6s^2$-$5p^5 4f^{14} 5d^{k+1}$ appear because of $5p^5 4f^{14} 5d^{k-1} 6s^2$ and $5p^5 4f^{14} 5d^k$ interactions, i.e., apparent two and three electron transitions can appear albeit weakly because of final-state configuration mixing. The single electron $5p$-$6s$ transitions are generally weaker than the $5p$-$5d$ within a given family of resonance, single $6s$ or double $6s$ satellites. The $5p$-$6s$ contributions in the latter two families are larger in terms of summed gf value purely as a result of the increased number of lines possible involving states with large J values. (2) All of the lines from the $5p$-$5d$, $6s$ transitions cover an energy range about two times wider than that for $4f$-$5d$ transitions. (3) All of the transition arrays have large average linewidths $\bar{\Gamma}$, which greatly exceed the instrumental resolution. As is indicated in Fig. 4, two strong and broad absorption features are predicted in the $5p$ excitation region. The distinct separation of the $5p$ excitations into two groups of resonances can be attributed to the spin-orbit splitting of the $5p$ hole. The first group of resonances around 58 eV can be ascribed to $5p_{3/2}$-$5d$ transitions; the second group, around 72 eV, is due to $5p_{1/2}$-$5d$ transitions. Furthermore,

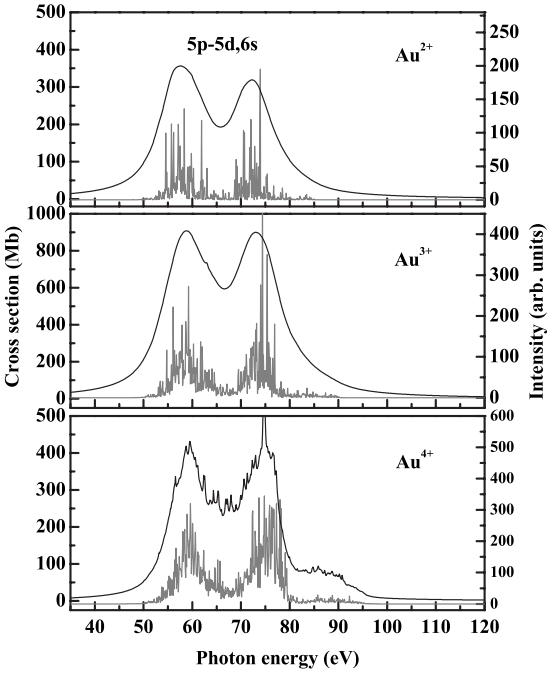

FIG. 4. Comparison between theoretical contributions of photoabsorption cross section (black lines) and line intensity (gray lines) due to $5p$-$5d$, $6s$ transition array of Au^{2+}, Au^{3+}, and Au^{4+}.

$5p_{3/2}$-$6s$ and $5p_{1/2}$-$6s$ transitions lie the higher energy side of two groups of resonances and make a significant contribution to the overall $5p$ photoabsorption profile. This type of spectral structure is very similar to the corresponding features in the spectra of atomic Lu and U [12,13]. In addition, in the calculations we also find that the structure of the $5p$-nd $(n \geq 6)$ array is very similar to that of the $5p$-$5d$ transition array, but the $5p$-nd $(n \geq 6)$ transitions are much weaker and can be neglected.

Based on the above analysis, we can see that the cross sections for photoexcitation from $4f$ and $5p$ subshells are overlapped in the energy region above 76 eV. Also the $4f$-nd transition arrays are superimposed on the high energy slopes of the cross section for $5p$-$5d$, $6s$ transition arrays.

IV. COMPARISON BETWEEN THEORETICAL AND EXPERIMENTAL SPECTRA

As already described, the characteristic features of the continuumlike structure from Au^{2+}, Au^{3+}, and Au^{4+} ions are readily observed and identified in the measured spectra. Since in laser-produced plasma thermalization times are some tens of picoseconds [14] absorption from excited terms of the ground configuration and lowest two configurations of each ion stage makes a sizable contribution to the overall photoabsorption spectrum. This effect, however, can be accounted for by assuming a normalized Boltzmann distribution among the ground terms, characteristic of a particular electron temperature. This procedure has already been shown to be successful in yielding good agreement between experiment and theory for the $4d$-np transitions in ionized Sn, Sb, Te, and Ba [15–17].

TABLE III. Theoretically calculated difference of configuration average energies between transitions (ΔE_{av}), energy range, number of lines (N), sum of gf values (Σgf), sum of weighted radiation probabilities (ΣgA^r), sum of autoionization probabilities (ΣgA^a), configuration average autoionization probabilities ($\bar{A}^a$), and average linewidths ($\bar{\Gamma}$) of each transition individual line of the $5p$-$5d$ in the spectra of Au^{2+}, Au^{3+}, and Au^{4+} ions. Numbers in brackets denote powers of 10.

Ions	Transition array	Energy range (eV)	N	Σgf	ΣgA^r (s^{-1})	ΣgA^a (s^{-1})	$\bar{A}^a$ (s^{-1})	$\bar{\Gamma}$ (eV)
Au^{2+}	$5p^64f^{14}5d^9$-$5p^54f^{14}5d^{10}$	54.55–70.73	3	7.10	1.18[12]	1.67[17]	1.67[16]	3.284
	$5p^64f^{14}5d^86s$-$5p^54f^{14}5d^{10}$	47.91–67.16	15	0.14	2.54[10]	8.00[17]	1.67[16]	3.418
	$5p^64f^{14}5d^76s^2$-$5p^54f^{14}5d^{10}$	37.41–60.23	7	0.04	5.86[09]	2.64[17]	1.65[16]	4.748
	$5p^64f^{14}5d^9$-$5p^54f^{14}5d^96s$	58.25–81.87	35	7.13	1.43[12]	2.59[18]	1.51[16]	2.057
	$5p^64f^{14}5d^86s$-$5p^54f^{14}5d^96s$	50.84–76.81	216	131.32	2.32[13]	1.65[19]	1.46[16]	1.904
	$5p^64f^{14}5d^76s^2$-$5p^54f^{14}5d^96s$	41.10–69.73	179	1.40	2.29[11]	1.40[19]	1.47[16]	1.877
	$5p^64f^{14}5d^9$-$5p^54f^{14}5d^86s^2$	63.88–91.58	43	0.17	3.85[10]	1.81[18]	8.08[15]	1.037
	$5p^64f^{14}5d^86s$-$5p^54f^{14}5d^86s^2$	56.20–86.94	390	36.46	7.65[12]	1.68[19]	7.64[15]	0.912
	$5p^64f^{14}5d^76s^2$-$5p^54f^{14}5d^86s^2$	46.74–80.18	460	273.57	5.08[13]	2.03[19]	7.55[15]	0.875
Au^{3+}	$5p^64f^{14}5d^8$-$5p^54f^{14}5d^9$	51.41–77.10	59	60.70	1.06[13]	4.20[18]	1.38[16]	1.815
	$5p^64f^{14}5d^76s$-$5p^54f^{14}5d^9$	40.88–69.61	190	2.00	3.39[11]	1.33[19]	1.32[16]	1.707
	$5p^64f^{14}5d^66s^2$-$5p^54f^{14}5d^9$	47.49–59.91	60	0.86	1.12[11]	4.05[18]	1.29[16]	1.637
	$5p^64f^{14}5d^8$-$5p^54f^{14}5d^86s$	57.30–88.11	385	34.73	7.66[12]	2.66[19]	1.22[16]	1.457
	$5p^64f^{14}5d^76s$-$5p^54f^{14}5d^86s$	46.56–81.23	1714	516.67	9.65[13]	1.22[20]	1.20[16]	1.372
	$5p^64f^{14}5d^66s^2$-$5p^54f^{14}5d^86s$	38.72–71.06	890	23.68	3.87[12]	6.67[19]	1.24[16]	1.364
	$5p^64f^{14}5d^8$-$5p^54f^{14}5d^76s^2$	67.41–101.37	309	6.70	1.60[12]	1.26[19]	7.01[15]	0.815
	$5p^64f^{14}5d^76s$-$5p^54f^{14}5d^76s^2$	55.60–95.04	1993	126.63	2.92[13]	8.29[19]	6.69[15]	0.729
	$5p^64f^{14}5d^66s^2$-$5p^54f^{14}5d^76s^2$	43.95–85.34	1671	627.93	1.25[14]	7.03[19]	6.67[15]	0.719
Au^{4+}	$5p^64f^{14}5d^7$-$5p^54f^{14}5d^8$	47.37–81.29	459	249.18	4.64[13]	3.85[19]	1.44[16]	1.661
	$5p^64f^{14}5d^66s$-$5p^54f^{14}5d^8$	39.66–71.16	831	19.20	3.11[12]	7.13[19]	1.43[16]	1.595
	$5p^64f^{14}5d^56s^2$-$5p^54f^{14}5d^8$	40.12–54.29	51	0.04	5.18[09]	4.70[18]	1.59[16]	1.707
	$5p^64f^{14}5d^7$-$5p^54f^{14}5d^76s$	57.33–94.96	1973	116.81	2.84[13]	5.82[19]	4.75[15]	0.520
	$5p^64f^{14}5d^66s$-$5p^54f^{14}5d^76s$	43.96–85.35	6231	1198.01	2.37[14]	1.89[20]	4.73[15]	0.504
	$5p^64f^{14}5d^56s^2$-$5p^54f^{14}5d^76s$	38.16–69.08	1767	49.85	8.06[12]	5.74[19]	4.96[15]	0.508
	$5p^64f^{14}5d^7$-$5p^54f^{14}5d^66s^2$	72.18–111.81	896	7.31	2.18[12]	5.63[18]	9.56[14]	0.099
	$5p^64f^{14}5d^66s$-$5p^54f^{14}5d^66s^2$	55.95–101.04	5075	263.36	6.74[13]	2.58[19]	7.79[14]	0.081
	$5p^64f^{14}5d^56s^2$-$5p^54f^{14}5d^66s^2$	44.43–85.07	3110	942.47	2.00[14]	1.58[19]	7.74[14]	0.080

In addition, to gain some insight into the plasma conditions, it is of interest to use the steady-state collisional-radiative (CR) model of Colombant and Tonon [18] to calculate the ion fractions of different ion stages as a function of n_e and T_e. If we define $P_{i,k}$ as the Boltzmann factor and F_i as the ion fraction for a range of electron temperatures for a given electron density, then based on Eq. (1), the total absorption cross section (in Mb) is defined by weighting and summing the corresponding Boltzmann factors and ion fractions for each ion to obtain an absorption profile,

$$\sigma_{\text{total}} = \sum_i F_i \sigma' = \sum_i F_i \{109.7\Gamma_{i,k}(f_{i,k}P_{i,k}) \times [2\pi(E_{i,k}-E)^2 + \Gamma_{i,k}^2/4]^{-1}\}. \quad (2)$$

In order to reproduce the experimental spectra, first, n_e was assumed to be 1×10^{21} cm^{-3} and the evolution of ion faction as a function of T_e was calculated based on the steady-state CR model. The total cross sections were then calculated using Eq. (2), and the results are presented in Fig. 5. In Fig. 5(a), the photoabsorption spectrum recorded at a time delay of 50 ns is compared with the results of theoretical calculations obtained for an electron temperature of 10 eV. It is seen that good agreement is obtained when the dominant fractional contribution arises from Au^{2+}, Au^{3+}, and Au^{4+} ions with values of 20%, 49%, and 27%, respectively. For clarity, Figs. 5(b)–5(d) also present the cross sections from Au^{2+}, Au^{3+}, and Au^{4+} ions by assuming a normalized Boltzmann distribution among the excited states for an electron temperature of 10 eV.

However, in the experimental setup the signal reaching the detector is the sum of signals from plasma volumes with different temperatures and densities and consequently a single plasma density or temperature cannot fully describe the ion populations. At the same time, due to the complexity of initial and final states considered in the calculations, it is

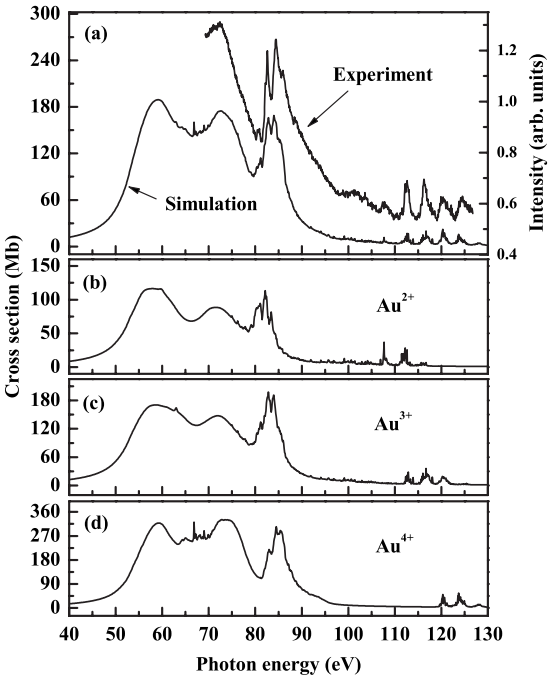

FIG. 5. Comparisons between the measured and simulated spectra. The total cross sections were calculated for each of the component terms of the ground and excited configurations of Au^{2+}, Au^{3+}, and Au^{4+}, then weighted and summed assuming a normalized Boltzmann distribution among the excited states and ion ratios obtained from the CR model by assuming an electron density of 1×10^{21} cm^{-3} to obtain an absorption profile. (a) The photoabsorption spectrum recorded at 50 ns time delays and the results of theoretical calculations for a given electron temperature of 10 eV. The dominant fractional contributions arise from Au^{2+}, Au^{3+}, and Au^{4+} ions are about 20%, 49%, and 27%, respectively. [(b)–(d)] The calculated cross sections by assuming a normalized Boltzmann distribution among the excited states for an electron temperature of 10 eV.

very difficult to accurately calculate the populations of energy levels. Hence, there are some discrepancies between the simulated and experimental spectra: (1) in the experimental results the intensity of the peak observed at 72.4 eV is higher than that of the peak at 82.4 eV, but in the simulated result, due to the overestimation of the contribution of $4f^{13}5d^{6}(4f,5p_{1/2}\text{-}5d)6s^{2}$ transition arrays of Au^{4+} ions which results directly from our single temperature plasma description, the intensity of the peak from the $5p_{1/2}$-$5d$, $6s$ transition arrays is almost equal to that of the peak from the $4f$-$5d$ transition arrays. (2) The intensity of the extended slope around 90 eV is lower in the simulated spectrum than the experimental one and originates from the omission of the higher-lying $5p$-nd ($n>5$) transitions and the effects of interference with the direct ionization of the $5d$ or $6s$ electrons into the same continuum states which will give rise to asymmetrical Fano resonances [19]. Moreover, a similar extended slope seen in the spectrum resulting from $5p$ photoabsorption in tungsten ions obtained by Costello *et al.* [6] was essentially reproduced in calculations for the $^{5}D_{0}$ ground-state spectrum of neutral tungsten by Boyle *et al.* [20] using many-body perturbation theory which explicitly allows for such interference effects within channels. (3) The intensities of the peaks in the 110–130 eV energy region are weaker than those seen in the experiment. In fact, the spectral features of the transition arrays $4f$-nd ($n>6$) are very similar to those of the $4f$-$6d$ and overlap one after another. However, because of computer memory limitation, those lines had to be neglected. The present differences indicate that we also underestimate the contribution of the higher-lying $4f$-nd ($n>6$) configurations. These discrepancies indicate that more detailed and accurate calculations should be needed, and this work is now in progress.

V. CONCLUSION

Photoabsorption spectra of Au^{2+}, Au^{3+}, and Au^{4+} ions have been observed in the 70–127 eV spectral region using the DLP technique. Calculations with the Cowan suite of codes were successful in accounting for all of the observed structure which arises from $4f$-$5d$, $6d$ transitions. Our calculations also predict the $5p$-$5d$, $6s$ transitions and find that the $4f$-nd transition arrays are superimposed on the high energy side of the $5p$-$5d$, $6s$ transition arrays. The present results show the importance of the satellite lines in the spectral profile and predict that the satellite lines from one and two $6s$ subshells are more important than resonance lines, and with increasing ionization, satellite contributions with one $6s$ spectator electron gradually become more important than those with two $6s$ spectator electrons.

Using the steady-state collisional-radiative model to simulate the observed spectra, we obtained good agreement with experiment under the conditions of electron temperature $T_e = 10$ eV and electron density $N_e = 1 \times 10^{21}$ cm^{-3}. Because there are still no experimental results for isolated highly charged gold ions, it is necessary to perform further experiments using merged beams to determine the spectral profile of the individual ions and to study the correlation satellites and the interaction of many discrete states with many continua. For isoelectronic comparison in this region, the spectra are expected to be dominated by the effects of $4f$ contraction and the fact that the $4f$ binding energy increases more rapidly than the $5p$ both with increasing Z and increasing ionic charge. Moreover, since the plasma temperatures required to produce these ions are relatively high, disentangling the contribution from ground-state absorption for isoelectronic comparison with data for neutral atoms from merged beam data where the absorption is generally confined to the lowest energy states can be difficult and any apparent agreement somewhat fortuitous. However it does give information on the relative separation of $4f$ and $5p$ levels. In the present case, Au^{2+} is isoelectronic with Ir whose experimental spectrum is dominated by two peaks of almost comparable amplitude due to $5p_{3/2}$-$5d$ and $4f$-$5d$ excitations [21]. The $4f$-$5d$ excitation essentially lies between a strong $5p_{3/2}$-$5d$ and a much weaker $5p_{1/2}$ array. Here in contrast, the $5p$ and $5f$ levels are well separated and the $4f$-$5d$ feature lies on the high energy side of the $5p_{1/2}$ excitation. For Au^{4+}, where the $4f$ and $5p$ features are even further separated the comparison is even more dramatic as in the isoelectronic atom, Re, the spectrum is dominated by intense structure due to the near

overlap of the $5p_{3/2}$ and $4f$ levels [22]. In Fig. 5 we present the resonant absorption cross sections from Au^{2+}, Au^{3+}, and Au^{4+}, which may be compared with T_e calculations in the above references and furthermore, we hope that the present results should be of use in forthcoming merged beam studies.

ACKNOWLEDGMENTS

This work has been supported by the National Natural Science Foundation of China (Grants No. 10774122 and No. 10876028), the China/Ireland Science and Technology Collaboration Research Fund (Grant No. CI-2004-07), the Specialized Research Fund for the Doctoral Program of Higher Education of China (Grant No. 20070736001), and the Foundation of Northwest Normal University (Grant No. NWNU-KJCXGC-03-21). Two of the authors (M.G.S. and C.Z.D.) would like to thank the School of Physics at UCD for their hospitality during their pleasant stay, while another (G.O'S.) would like to acknowledge the exceptional hospitality of staff and students at NWNU.

[1] M. J. May, K. B. Fournier, P. Beiersdorfer, H. Chen, and K. L. Wong, Phys. Rev. E **68**, 036402 (2003).
[2] S. H. Glenzer, K. B. Fournier, B. G. Wilson, R. W. Lee, and L. J. Suter, Phys. Rev. Lett. **87**, 045002 (2001).
[3] M. E. Foord, S. H. Glenzer, R. S. Thoe, K. L. Wong, K. B. Fournier, B. G. Wilson, and P. T. Springer, Phys. Rev. Lett. **85**, 992 (2000).
[4] K. Honda, K. Mima, and F. Koike, Phys. Rev. E **55**, 4594 (1997).
[5] R. Haensel, K. Radler, and B. Sonntag, Solid State Commun. **7**, 1495 (1969).
[6] J. T. Costello, E. T. Kennedy, B. F. Sonntag, and C. L. Cromer, J. Phys. B **24**, 5063 (1991).
[7] U. Koble, J. T. Costello, J. P. Mosnier, E. T. Kennedy, and M. Martins, J. Phys. B **28**, 181 (1995).
[8] A. Zangwill and D. A. Liberman, Comput. Phys. Commun. **32**, 63 (1984).
[9] J. T. Costello, E. T. Kennedy, J. P. Mosnier, P. K. Carroll, and G. O'Sullivan, Phys. Scr. **T34**, 77 (1991).
[10] E. T. Kennedy, J. T. Costello, J. P. Mosnier, and P. van Kampen, Radiat. Phys. Chem. **70**, 291 (2004).
[11] R. D. Cowan, *The Theory of Atomic Structure and Spectra* (University of California Press, Berkeley, 1981).
[12] Ch. Gerth, B. Kanngießer, M. Martins, P. Sladeczek, K. Tiedtke, and P. Zimmermann, Eur. Phys. J. D **5**, 65 (1999).
[13] P. van Kampen, Ch. Gerth, M. Martins, P. K. Carroll, J. Hirsch, E. T. Kennedy, O. Meighan, J.-P. Mosnier, P. Zimmermann, and J. T. Costello, Phys. Rev. A **61**, 062706 (2000).
[14] D. Salzmann, *Atomic Physics in Hot Plasmas* (Oxford University Press, Oxford, 1998).
[15] M. A. Lysaght, D. Kilbane, A. Cummings, N. Murphy, P. Dunne, G. O'Sullivan, P. van Kampen, J. T. Costello, and E. T. Kennedy, J. Phys. B **38**, 4247 (2005).
[16] N. Murphy, J. T. Costello, E. T. Kennedy, C. McGuinness, J. P. Mosnier, B. Weinmann, and G. O'Sullivan, J. Phys. B **32**, 3905 (1999).
[17] N. Murphy, P. Niga, A. Cummings, P. Dunne, and G. O'Sullivan, J. Phys. B **39**, 365 (2006).
[18] D. Colombant and G. F. Tonon, J. Appl. Phys. **44**, 3524 (1973).
[19] U. Fano, Phys. Rev. **124**, 1866 (1961).
[20] J. J. Boyle, Z. Altun, and H. P. Kelly, Phys. Rev. A **47**, 4811 (1993).
[21] M. Martins, P. Sladeczek, K. Tiedtke, and P. Zimmermann, Phys. Rev. A **55**, R8 (1997).
[22] M. Martins, P. Sladeczek, K. Tiedtke, and P. Zimmermann, Phys. Rev. A **56**, 1329 (1997).